Mechanisms of the Great Plains Low-Level Jet as Simulated in an AGCM

XIANAN JIANG

Atmospheric and Oceanic Sciences Program, Princeton University, Princeton, New Jersey

NGAR-CHEUNG LAU, ISAAC M. HELD, AND JEFFREY J. PLOSHAY

NOAA/Geophysical Fluid Dynamics Laboratory, Princeton University, Princeton, New Jersey

ABSTRACT

A model diagnosis has been performed on the nocturnal Great Plains low-level jet (LLJ), which is one of the key elements of the warm season regional climate over North America. The horizontal–vertical structure, diurnal phase, and amplitude of the LLJ are well simulated by an atmospheric general circulation model (AGCM), thus justifying a reevaluation of the physical mechanisms for the formation of the LLJ based on output from this model. A diagnosis of the AGCM data confirms that two planetary boundary layer (PBL) processes, the diurnal oscillation of the pressure gradient force and of vertical diffusion, are of comparable importance in regulating the inertial oscillation of the winds, which leads to the occurrence of maximum LLJ strength during nighttime. These two processes are highlighted in the theories for the LLJ proposed by Holton (1967) and Blackadar (1957). A simple model is constructed in order to study the relative roles of these two mechanisms. This model incorporates the diurnal variation of the pressure gradient force and vertical diffusion coefficients as obtained from the AGCM simulation. The results reveal that the observed diurnal phase and amplitude of the LLJ can be attributed to the combination of these two mechanisms. The LLJ generated by either Holton's or Blackadar's mechanism alone is characterized by an unrealistic meridional phase shift and weaker amplitude.

It is also shown that the diurnal phase of the LLJ exhibits vertical variations in the PBL, more clearly at higher latitudes, with the upper PBL wind attaining a southerly peak several hours earlier than the lower PBL. The simple model demonstrates that this phase tilt is due mainly to sequential triggering of the inertial oscillation from upper to lower PBL when surface cooling commences after sunset. At lower latitudes, due to the change of orientation of prevailing mean wind vectors and the longer inertial period, the inertial oscillation in the lower PBL tends to be interrupted by strong vertical mixing in the following day, whereas in the upper PBL, the inertial oscillation can proceed in a low-friction environment for a relatively longer duration. Thus, the vertical phase tilt initiated at sunset is less evident at lower latitudes.

1. Introduction

During the summer months from April to September, the Great Plains of the United States are characterized by the frequent occurrence of a southerly low-level jet (LLJ). This LLJ is mainly confined in the boundary layer with maximum wind speeds typically at 500–1000 m above the ground. The jet exhibits strong diurnal oscillation, with the strongest wind speed mostly occurring during the night. This Great Plains LLJ has been intensively documented during the past decades (e.g., Means 1952, 1954; Hering and Borden 1962; Izumi and Barad 1963; Hoecker 1963, 1965; Parish et al. 1988; Frisch et al. 1992; Mitchell and Arritt 1995; and many others). Bonner (1968) provides a comprehensive study on the climatology of the LLJ.

The nocturnal LLJ could play an active role in modulating the diurnal cycle of summertime rainfall over the Great Plains, where the deep convection exhibits a midnight/early morning maximum, in stark contrast to the afternoon rainfall peak observed over most inland regions. The low-level convergence at the nose of the jet axis and cyclonic vorticity to the left of the jet center are conducive to the formation of deep convection (Pitchford and London 1962; Means 1954; Astling et al.

Corresponding author address: Dr. Xianan Jiang, USDOC/NOAA/GFDL, P.O. Box 308, 201 Forrestal Rd., Princeton, NJ 08542.
E-mail: xianan.jiang@noaa.gov

1985; McCorcle 1988). In addition, moisture transport from the Gulf of Mexico to the Great Plains by the nocturnal jet provides a preferred environment for deep convection (Benton and Estoque 1954; Rasmusson 1967, 1968; Wallace 1975; Helfand and Schubert 1995; Higgins et al. 1997). The LLJ is also important to the development of mesoscale convective complexes by supplying warm, moist air (Maddox 1980). Ting and Wang (2006) show that the interannual variability of rainfall over the continental United States, for instance, the 1988 drought and the 1993 flood, is tightly related to the strength of the summer mean LLJ. The LLJ is therefore a critical entity in the regional climate system over the U.S. continent during summer.

Two well-known theories for the LLJ emphasize processes in the planetary boundary layer (PBL). Blackadar (1957) proposed that the formation of the LLJ during the night is caused by an inertial oscillation, triggered by the sudden reduction in eddy viscosity at sunset due to stabilization of the PBL resulting from radiative cooling of the land surface. However, this theory does not explain the preferred occurrence of the LLJ over the Great Plains. Another theory by Holton (1967), based upon the original suggestion by Bleeker and Andre (1951), highlighted the important role of the diurnal buoyancy-driven flow over the sloping terrain of the Rockies in forcing the nocturnal LLJ over the Great Plains.

While these theories emphasize the role of PBL processes for the LLJ, Wexler (1961) proposed that the LLJ results from the blocking effect by the Rockies when the Bermuda high extends westward to this region, analogous to the formation of western boundary currents in the ocean. This mechanism may contribute to the summer mean southerly flow over this region as illustrated by Ting and Wang (2006); however, it does not explain the strong diurnal oscillation of the jet. Uccellini and Johnson (1979) related the synoptic variability of the LLJ to the interaction between upper-level jet streaks and diabatic processes associated with cyclogenesis.

The LLJ has been simulated and analyzed in many studies based on a variety of models (Krishna 1968; Bonner and Paegle 1970; McNider and Pielke 1981; Paegle and McLawhorn 1983; Astling et al. 1985; McCorcle 1988; Fast and McCorcle 1990; Zhong et al. 1996; Helfand and Schubert 1995; and others). Most of these studies were based on idealized 1D or 2D models, and the relative importance of various mechanisms for the observed LLJ has not been definitively illustrated.

Capitalizing on the recent release of high-resolution North American Regional Reanalysis (NARR) and the new-generation atmospheric general circulation model (AGCM) at the Geophysical Fluid Dynamics Laboratory (GFDL), we have made an attempt to understand the relative importance of the physical processes responsible for the formation of the LLJ based on a successful simulation of the LLJ by the AGCM. The organization of this paper is as follows. The regional reanalysis dataset and AGCM employed in this study are described in section 2. In section 3, we compare AGCM-simulated features of the LLJ with the observations based on regional reanalysis data. Then the physical mechanisms responsible for the formation of the LLJ are examined using a simplified model driven by diurnal forcing from the AGCM simulation. Finally, a summary and discussion are presented.

2. Data and model

a. North American Regional Reanalysis

The primary observational dataset used for this study is the North American Regional Reanalysis (Mesinger et al. 2006). It is a long-term (25 yr from October 1978 to December 2003), consistent, high-resolution (32 km, 45 layer, 3 hourly) climate dataset for North America. This product is compiled using the National Centers for Environmental Prediction (NCEP) mesoscale Eta forecast model and its data assimilation system. In particular, the precipitation field in this dataset is in good agreement with observations. Temperature and vector wind are also considerably improved over the corresponding fields in the global NCEP reanalysis throughout the troposphere; such improvements are especially notable for the 2-m temperature and 10-m winds. Detailed information on the dataset can be found online (see http://www.emc.ncep.noaa.gov/mmb/rreanl/index.html).

In this study, the NARR is employed to assess the AGCM performance in simulating summer mean circulation and climatological features of the LLJ, including its diurnal phase and amplitude. The regional reanalysis precipitation and moisture fields are also used to demonstrate the intimate association between the nocturnal rainfall and moisture transport by the LLJ over the Great Plains. For this purpose, 3-hourly data including wind, specific humidity at 29 pressure levels, as well as precipitation rate for each day in June, July, and August from 1979 to 2003 are averaged to obtain a 3-hourly summertime climatological diurnal cycle.

b. GFDL AGCM

The global atmosphere and land model developed by the GFDL Global Atmospheric Model Development Team (2004) is used for this study. This model uses a

finite-difference formulation. The latitude–longitude horizontal grid is the staggered Arakawa B grid with a resolution of 1° latitude × 1.25° longitude; this is a factor of 2 higher in resolution than the version described by the GFDL Global Atmospheric Model Development Team (2004). A sigma-pressure hybrid vertical coordinate is adopted. There are 24 vertical levels. Nine of these levels are located in the lowest 1.5 km above the surface. Diurnal changes in radiative transfer are incorporated in the model. Moist convection is represented by the relaxed Arakawa–Schubert scheme (Moorthi and Suarez 1992). The detailed dynamical and physical components of this atmosphere–land model, as well as its capability of simulating various aspects of the climate system, can be found in the manuscript by the GFDL Global Atmospheric Model Development Team (2004). Considering that the LLJ is primarily a phenomenon occurring in the PBL, some details of the PBL scheme in the AGCM are provided below.

1) SURFACE FLUXES

Surface fluxes are computed using the Monin–Obukhov similarity (MOS) theory. The key assumption in MOS is that the wind (u) and buoyancy (b) profiles are dependent on $\zeta = z/L$, where z is the height and L is the Monin–Obukhov length, that is,

$$\frac{kz}{u_*}\frac{\partial u}{\partial z} = \Phi_m(\zeta) \tag{1}$$

$$\frac{kz}{b_*}\frac{\partial b}{\partial z} = \Phi_b(\zeta) \tag{2}$$

where k is von Kármán's constant, u_* and b_* are the frictional velocity and buoyancy scales, respectively, and $\Phi_m(\zeta)$ and $\Phi_b(\zeta)$ are stability functions for the momentum and buoyancy fluxes, respectively, which are given as the following forms.

For unstable cases ($\zeta < 0$),

$$\Phi_m = (1 - 16\zeta)^{-1/4} \tag{3}$$

$$\Phi_b = (1 - 16\zeta)^{-1/2}. \tag{4}$$

To recognize the contribution of subgrid-scale wind fluctuations to surface fluxes, a gustiness component that is proportional to the surface buoyancy flux (Beljaars 1995) is incorporated into the wind speed when calculating the fluxes.

And for the stable case ($\zeta > 0$),

$$\Phi_m = \Phi_b = 1 + 5\zeta; \quad \zeta < \zeta_T; \tag{5}$$

$$\Phi_m = \Phi_b = 1 + (5 - \beta)\zeta_T + \beta\zeta; \quad \zeta \geq \zeta_T; \tag{6}$$

where β controls the critical Richardson number ($\beta = 1/\mathrm{Ri}_{cr}$) and ζ_T controls the point at which a transition is made from the established empirical stability function for the fully turbulent boundary layer to the presumably intermittent turbulence at high stability in order to enhance the drag coefficients for Richardson numbers in excess of 0.2. This treatment prevents the decoupling of the surface temperature from that of the atmosphere in highly stable conditions. In the current model, β is set to be 0.1, and ζ_T to be 0.5. Oceanic roughness lengths for momentum, heat, and moisture are prescribed according to Beljaars (1995).

2) VERTICAL DIFFUSION

Vertical diffusion coefficients are computed based on a K-profile scheme following Lock et al. (2000). Both convective boundary layers and near-surface convective layers driven by strong radiative cooling from cloud tops are considered in the model. First, any unstable layers are identified and classified so as to distinguish between those that are well mixed (clear and stratocumulus-capped layers) and those in which cumulus convection is present. Entrainment at the top of well-mixed layers is parameterized directly using the scheme by Lock (1998). When calculating the diffusivity for the interior layers, the nonlocal scheme by Lock et al. (2000) is used for the turbulence driven from the cloud top. For the surface-driven turbulence, a local K-scheme with Richardson number–based Monin–Obukhov stability function based on Eqs. (3)–(4) is employed in the AGCM. Additionally, the impact of cumulus convection on the horizontal momentum fields is considered by adding a component to the vertical diffusion coefficient for momentum. This component is proportional to the total cumulus mass flux predicted by the convection scheme.

For layers of the atmosphere that are not part of either a convective PBL or a stratocumulus layer, a local mixing parameterization scheme based on Louis (1979) is applied for the unstable layers. For stable layers, the diffusivity is calculated by a local K-scheme with stability function derived by Eqs. (5)–(6) and smoothly transited to that above the surface layer, which is formulated using the traditional form, with no mixing when the Richardson number exceeds 0.2.

Two experiments are conducted using this AGCM. In the control experiment, the default setting of physical parameters as well as the global orography are adopted. In the second experiment (AGCM_NOTP), the physical parameters are the same as the control run, but the global topography is replaced by a flat land
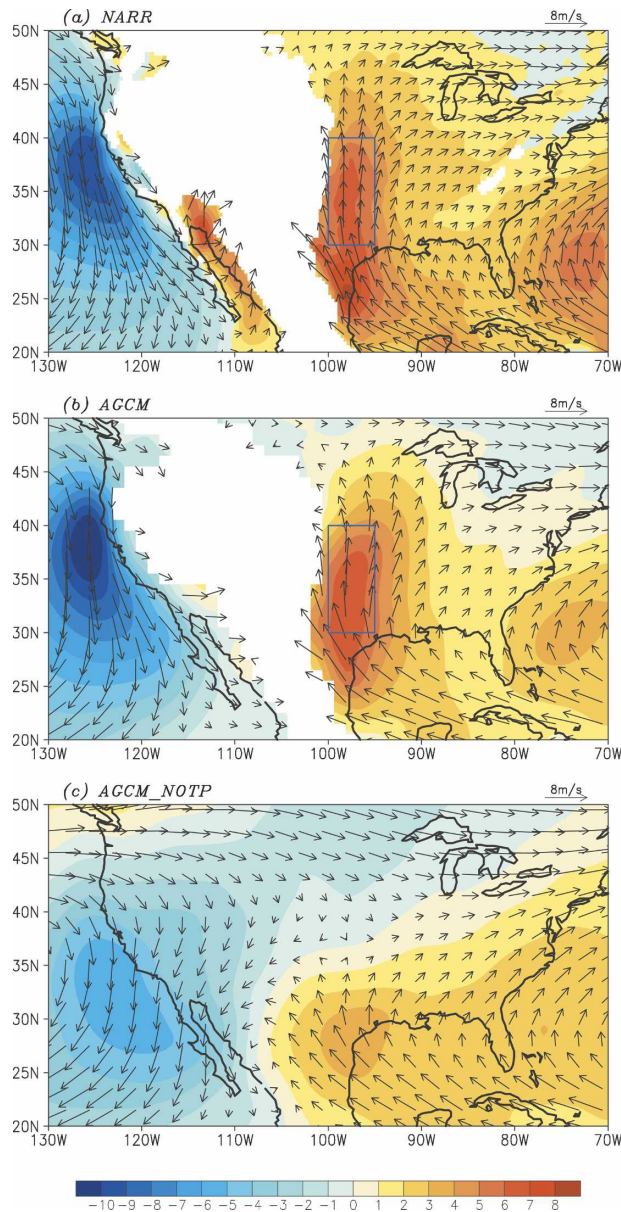
FIG. 1. Summer mean wind vectors (arrows; see scale at upper rhs) at 925 mb for (a) NARR, (b) AGCM control run, and (c) AGCM with global orography removed. The colors indicate the meridional wind component [scale bar at bottom (m s^{-1})]. The rectangular box in (a) and (b) indicates the LLJ region.

surface. Both of the experiments are integrated for 5 yr and hourly output is archived. The climatological diurnal cycle and summer mean patterns are calculated based on 3 summer months (June–August) within the 5-yr duration.

3. AGCM-simulated LLJ

Figures 1a–c show the climatological summertime daily averaged wind pattern at 925 mb by the NARR, AGCM, and AGCM with topography removed (AGCM_NOTP), respectively. The color shading in each represents the amplitude of the meridional wind component. In the regional reanalysis (Fig. 1a), the summertime low-level circulation over North America is characterized by two subtropical highs over the Pacific and Atlantic Oceans. Associated with Pacific subtropical highs, a strong northerly jet (California jet) is discerned over the Pacific Ocean off the coast of California. Meanwhile, a strong southerly jet is detected over the Great Plains, stretching from the Gulf of Mexico to South Dakota. The maximum southerly wind of the LLJ is confined to a narrow region between 100° and 95°W. The main features of this low-level circulation are well simulated by the AGCM (Fig. 1b), including the location and amplitudes of two subtropical highs and the Great Plains LLJ. The amplitude of simulated southerly wind associated with the Atlantic High is weaker than observed. The maximum wind center over the Gulf Coast at 25°N in the regional reanalysis is not captured by the AGCM simulation. In the AGCM_NOTP experiment (Fig. 1c), the amplitudes of the two subtropical highs are greatly reduced. The southerly LLJ over the Great Plains as noted in the reanalysis and control AGCM run are not detected in this case and only weak southerly wind is present over the Gulf Coast. These results are consistent with those reported by Ting and Wang (2006), who examined the summer mean pattern at 850 mb in the same AGCM with 2° × 2.5° resolution.

Figure 2 displays the diurnal veering of 925-mb wind vectors over the Great Plains at 3-hourly intervals. The daily mean wind over each grid point has been removed to highlight the diurnal oscillating component. Figure 2a shows the results in the NARR. Strong diurnal oscillation of the wind is readily seen over the LLJ region. The maximum amplitude is found between 100° and 95°W, where the maximum southerly jet is observed in the mean circulation (Fig. 1a). The perturbation wind exhibits a clockwise rotation with time and is indicative of an inertial oscillation. A maximum southerly wind component tends to occur at night between 0000 and 0300 local time (LT). This nocturnal southerly perturbation wind component tends to enhance the mean southerly flow and leads to a strong LLJ. During daytime from 1200 LT to 2100 LT, the amplitude of the perturbation wind is weaker than during nighttime and is directed southward; that is, the mean southerly flow is weakened during this period. All these features are very well captured by the AGCM simulation (Fig. 2b). The simulated perturbation wind exhibits slightly stronger diurnal amplitude, and the strong diurnal signal extends more eastward and less northward compared to
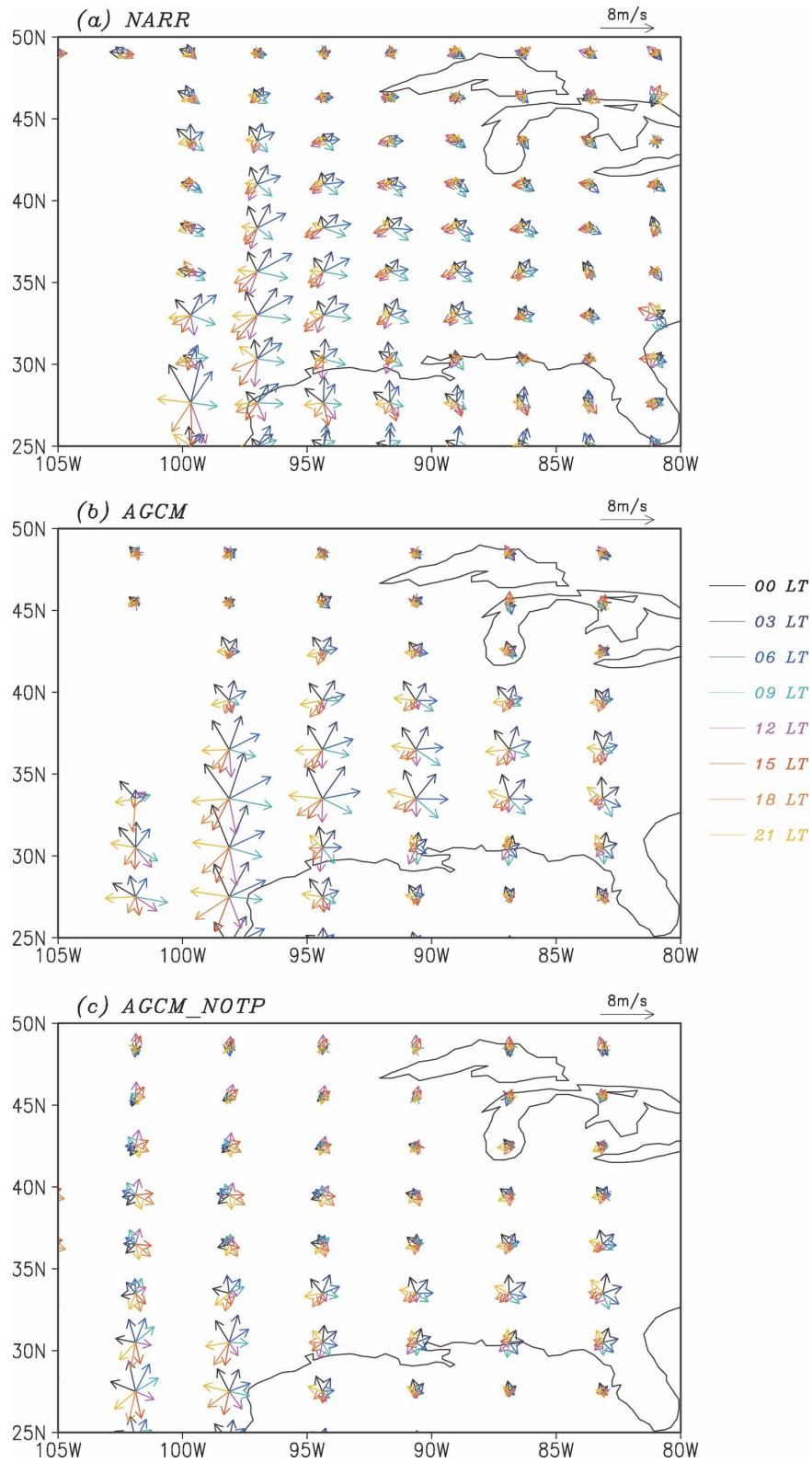
FIG. 2. Diurnal cycle of the perturbation wind vector at 925 mb at 3-h intervals for (a) NARR, (b) AGCM control run, and (c) AGCM with global orography removed. The scale of vectors is given at the upper rhs for each. Wind vectors at various times of the day are shown according to the color scheme shown on the rhs.
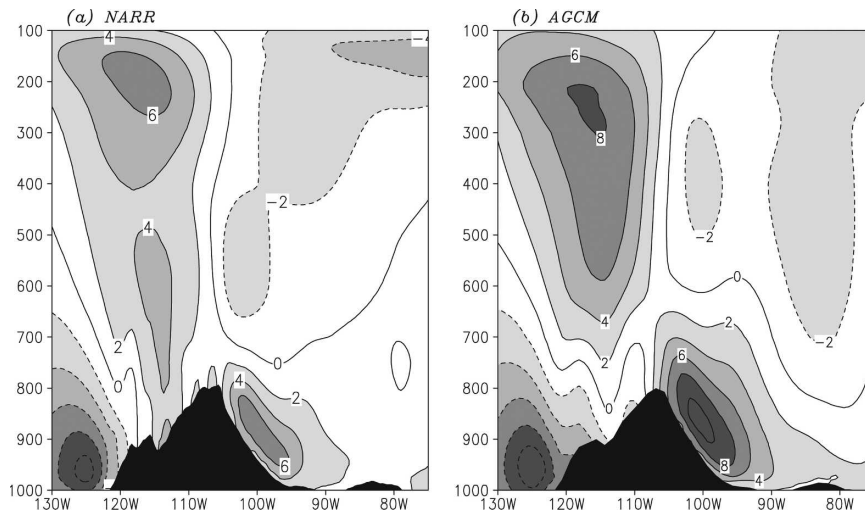
FIG. 3. Longitude–pressure distributions of the meridional wind component at 0300 LT [scale bar at bottom (m s^{-1})] for (a) NARR and (b) AGCM. The topography is indicated using dark shading. Both the wind data and orography are averaged over the latitudes from 30° to 40°N.

the reanalysis. The simulation by the AGCM experiment without topography has a totally different character. The maximum diurnal wind amplitude is mainly located near the coastal regions; the signal is rather weak compared to the reanalysis and AGCM control run over the Great Plains.

The above results confirm that the formation of the LLJ is closely associated with topography over North America. The intimate relationship between the LLJ and topography is further illustrated by the vertical–longitudinal profile of meridional wind at 0300 LT based on the NARR (Fig. 3a) and AGCM control run (Fig. 3b). The wind data are averaged between the 30°–40°N zone, which corresponds to the location of the LLJ centers. The selection of 0300 LT is based on the consideration that the peak of the LLJ is detected at this time (Fig. 2). (Hereafter, the term "AGCM" denotes the AGCM control run unless indicated otherwise.) In Fig. 3, the northerly California Jet over the Pacific Ocean and the southerly LLJ over the Great Plains are readily discerned in both the NARR reanalysis and AGCM simulation. The LLJ center is located on the slope of the Rockies in both Figs. 3a,b. A reversed circulation with a northerly wind component is found above the LLJ at about 100°W. A large anticyclone over the mountain region in the upper troposphere is discerned in both the NARR and AGCM. The amplitude of the LLJ is slightly stronger in the AGCM simulation compared to that in the reanalysis. The LLJ is also more confined to the surface in the NARR. The northerly wind center above the jet is located between

500 and 600 mb in the NARR, whereas it appears at about 400 mb in the AGCM simulation.

Figure 4 portrays the diurnal evolution of the meridional wind at various levels over the region 30°–40°N, 100°–95°W (see box in Fig. 1). The diurnal phase of the LLJ is very well captured by the AGCM despite the fact that the simulated LLJ has a greater vertical extent, and its amplitude is stronger than that in the reanalysis. Consistent with the reanalysis and many previous observational studies, the peak of the LLJ southerlies appears at about 0200 LT, with the maximum center located at about 900 mb (i.e., 600 m above ground level). Another noteworthy feature illustrated by both the NARR and AGCM is that the aforementioned reversed circulation in the middle troposphere over the LLJ also exhibits a clear diurnal oscillation. This upper-level center is situated relatively higher in the AGCM simulation. This out-of-phase diurnal oscillation between the low-level and upper-level wind field has also been reported by Hering and Borden (1962; station observation), Helfand and Schubert (1995; AGCM simulation) and Higgins et al. (1997; profiler observation). Helfand and Schubert (1995) ascribed this phenomenon to a "thermal chimney" effect, in which daytime heating/nighttime cooling over the high terrain plays an important role for the out-of-phase diurnal oscillation between low-level and upper-level wind.

In summary, the AGCM is capable of simulating most of the important features of the LLJ, including its horizontal and vertical structures and its diurnal evolu-
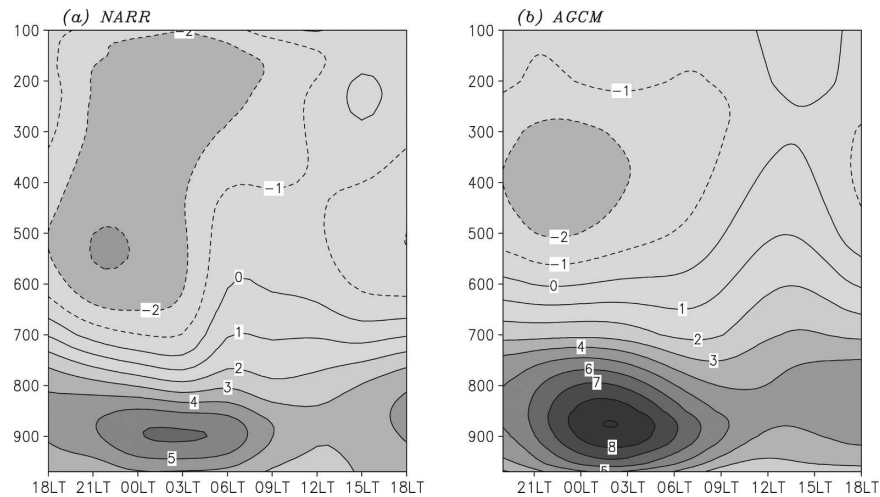
FIG. 4. Vertical distribution of the diurnal evolution of the meridional wind component (m s^{-1}) for (a) NARR and (b) AGCM. The wind data are averaged over the box region (30°–40°N, 100°–95°W) shown in Fig. 1.

tion. The results confirm that the LLJ is closely associated with the orography of North America.

4. Mechanisms for the LLJ

a. Diurnal forcing for the LLJ

To explore the mechanisms for the formation of the nocturnal LLJ, we will start with the following momentum equation with standard notations,

$$\frac{\partial \mathbf{V}}{\partial t} = \underbrace{-f \cdot \mathbf{k} \times \mathbf{V}}_{(I)} \underbrace{- \frac{1}{\rho} \boldsymbol{\nabla} p}_{(II)} + \underbrace{\frac{\partial}{\partial z}\left(K_d \frac{\partial \mathbf{V}}{\partial z}\right)}_{(III)} + \underbrace{\text{residual.}}_{(IV)}$$

(7)

The Coriolis force (I) generates an inertial oscillation, which has been found to be important for the LLJ by many previous studies and by the results presented in the last section. The key question is how this inertial oscillation is forced and its phase determined.

One external forcing contributing to the formation of the LLJ has been proposed by Holton (1967). This mechanism hinges on the diurnal variation of the pressure gradient force (II) caused by the alternative heating and cooling over sloping terrain. Based on Holton's argument, radiative heating over the mountain region during the afternoon results in an upslope pressure gradient force, which leads to westward tendencies over the east side of the mountain range. This westward wind component undergoes a clockwise rotation in accordance with the inertial oscillation and acquires a southerly component several hours later (i.e., near midnight). Conversely, inertial oscillation of the wind

changes induced by the radiative cooling during nighttime leads to a northerly component near noon. Since summer mean low-level wind over the Great Plains is southerly, the mean circulation is enhanced during nighttime and weakened during daytime. This mechanism thus explains the preferred occurrence of the LLJ over the eastern scope of the Rockies during nighttime.

The longitude–pressure distribution of the geopotential height (shading) and temperature (contours) fields at 1800 LT based on NARR and AGCM data are shown in Figs. 5a,b. The daily mean of both fields have been removed to emphasize the diurnal oscillating component. The most prominent feature for the observed geopotential height over the mountain region (Fig. 5a) is the negative perturbation near the surface, with the minimum being located over mountain top (105°W) and positive perturbation above 600 mb over the mountain. A similar pattern over the mountain region is reproduced by the AGCM (Fig. 5b), although some deficiencies do exist for other regions (e.g., the Pacific subtropical region between 130° and 120°W). In conjunction with the negative/positive perturbation geopotential height in the lower/upper troposphere over the mountain region, positive temperature perturbations prevail in that region in both the NARR and AGCM results. These temperature changes attain maximum amplitude near the surface and extend upward to the midtroposphere. This vertical profile is indicative of daytime radiative heating of the surface. In the AGCM, this positive temperature perturbation is mainly caused by the vertical mixing of sensible heat from the ground surface, in accord with the thermal chimney noted by Helfand and Schubert (1995).
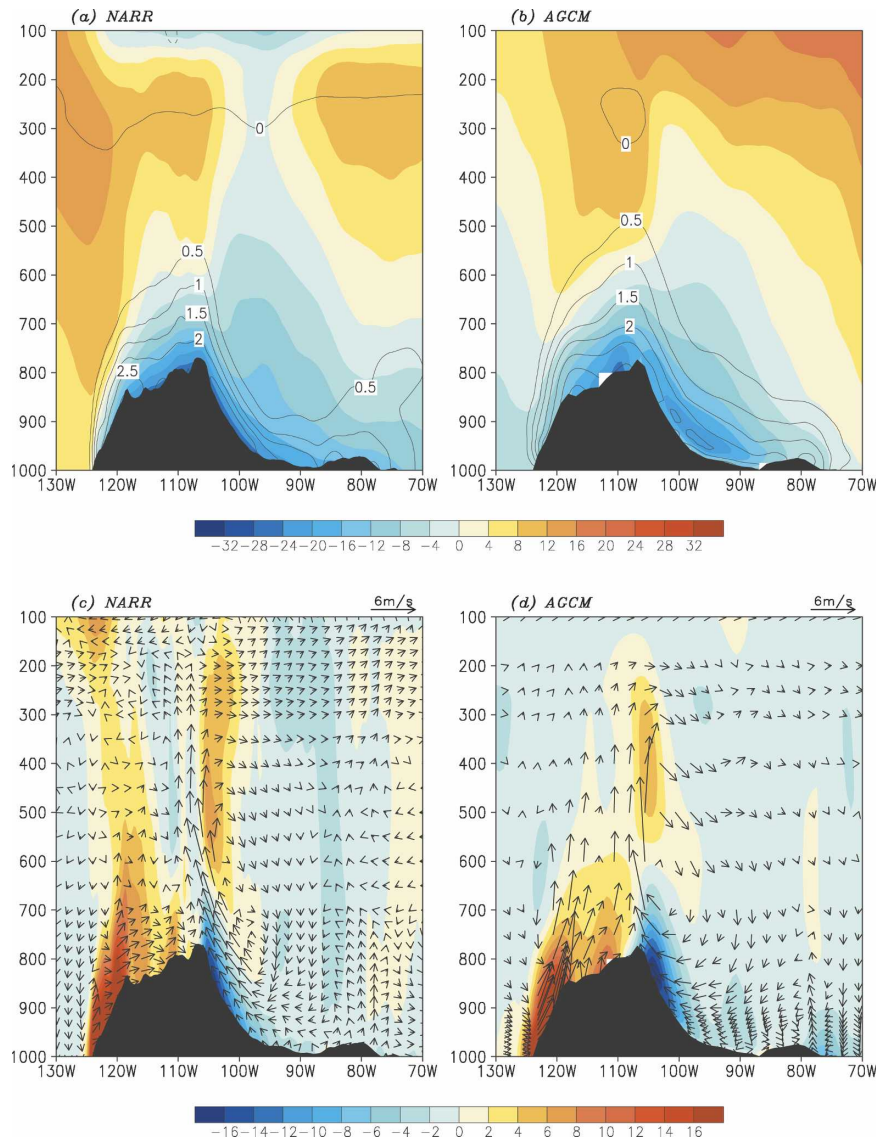
FIG. 5. Longitude–pressure distributions at 1800 LT of the perturbation geopotential height (shading; see scale bar; units: gpm) and air temperature [contours (K)] for (a) NARR and (b) AGCM and of perturbation zonal pressure gradient force [shading; see scale bar (m s^{-1})] and wind vectors on zonal-vertical plane [arrows; see scale at upper rhs (m s^{-1}) for u and 50 Pa s^{-1} for ω] for (c) NARR and (d) AGCM. All variables are averaged over the latitudes from 30° to 40°N.

Figures 5c,d portray the zonal pressure gradient force (shading) and airflow on the zonal plane (vectors) based on NARR (Fig. 5c) and AGCM (Fig. 5d) data. Again, only the diurnal perturbation component is shown for both fields. As shown in Fig. 5c, the negative pressure gradient is found on the eastern slope of the mountain (105°–100°W), and the positive pressure gradient force over the western side, consistent with the geopotential height pattern in Fig. 5a. A reversed pattern of the pressure gradient force in the mid- to upper troposphere is noticed over the mountain

peak (105°W). Associated with this pressure gradient pattern, upslope winds prevail on both sides of the mountain, with higher speeds on the eastern side. Strong upward motion and a divergent flow pattern around 300 mb are discernible at 105°W. Also evident is the weak downward motion to the east of the mountain. This subsidence in the afternoon over the Great Plains could suppress daytime rainfall and has been noted as a possible factor responsible for the nocturnal peak of rainfall over this region (e.g., Wallace 1975).

All of the above features can also be detected in the AGCM simulation (Fig. 5d). The westward-directed pressure gradient force over the eastern slope of the mountain at a low level is more confined to the surface in NARR than in the AGCM. Moreover, the altitude of strongest positive pressure gradient force in the middle and upper troposphere is higher in the AGCM (400 mb) than that in NARR. This discrepancy in the pressure gradient field is consistent with that of the wind fields as discussed in Figs. 3 and 4. The pressure gradient patterns in Figs. 5c,d are linked to the heating profile over the mountain region, which may be inferred from the temperature distributions in Figs. 5a,b. The heating as simulated in the AGCM is characterized by broader horizontal and vertical extents, which could result from model exaggeration of the surface sensible heat flux due to the known summertime warm and dry bias over the Great Plains in this AGCM (Klein et al. 2006). The accuracy of the vertical diffusion scheme also needs to be tested more carefully. Also, it is worth noting that while the surface sensible heat dominates in producing this mountain/plain circulation, the latent heat release associated with the convection near the top of the Rockies during daytime may further enhance this circulation.

To further illustrate the intimate relationship between the topography and perturbation wind component, Figs. 6a,b show the surface wind field over the mountain region at 2100 LT based on reanalysis and AGCM data, respectively. It is readily seen from both figures that the perturbation diurnal wind component displays a clear upslope motion and converges to the peaks of the Rocky Mountain ranges. The higher resolution in the reanalysis yields more detailed features in the circulation pattern.

The perturbation pressure gradient and circulation patterns (not shown) during nighttime are opposite to their daytime counterparts (Figs. 5, 6). These results are in support of the mechanism of the LLJ as proposed by Holton (1967).

Another mechanism for LLJ formation is associated with the sharp diminution of friction at sunset, as argued by Blackadar (1957). During daytime, due to the radiative heating over land surface, thermally driven vertical mixing is strong and extends through a thick atmospheric column, thereby exerting a considerable damping effect in the PBL. After sunset, the PBL is stabilized by the radiative cooling at the land surface, thus resulting in marked reduction in vertical mixing and a very shallow PBL. Since friction always acts in a direction opposite to that of the airflow, and given that the daily mean flow is northward, the reduced friction at nighttime would lead to increased northward ten-
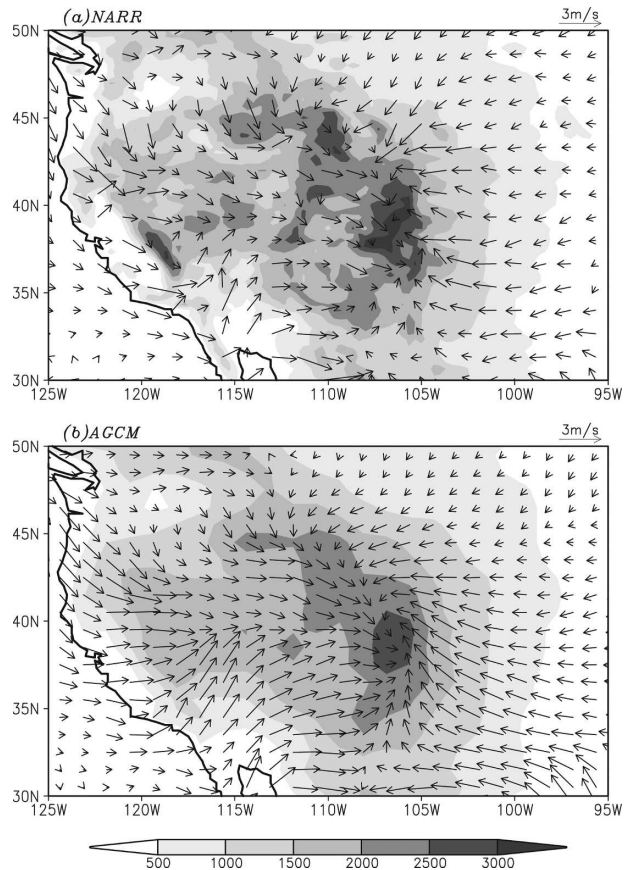

FIG. 6. Surface wind vectors at 2100 LT (see scale at upper rhs) for (a) NARR and (b) AGCM. The shading indicates the topography [scale bar at bottom (m)].

dency while the enhanced friction during daytime would give rise to southward tendency through the third term on the rhs of Eq. (7). Thus, an inertial oscillation is sustained and a southerly jet tends to form during the night.

In Fig. 7, the diurnal evolution of the vertical diffusion and surface drag coefficients are displayed using AGCM data, as averaged over the LLJ center. The air in the PBL experiences very strong vertical diffusion and surface drag during daytime, while both coefficients are greatly reduced during nighttime. These results are consistent with Blackadar's argument.

To determine the relative importance of processes for the formation of the LLJ, we conduct a budget analysis based on Eq. (7) with the AGCM output. The analysis confirms the expectation that the residual term is small in comparison to the first three terms on the rhs of Eq. (7) (figures not shown). While the total tendency for the diurnal variation of the horizontal wind is largely contributed by the Coriolis force (inertial oscillation), the wind tendencies associated with the diurnal
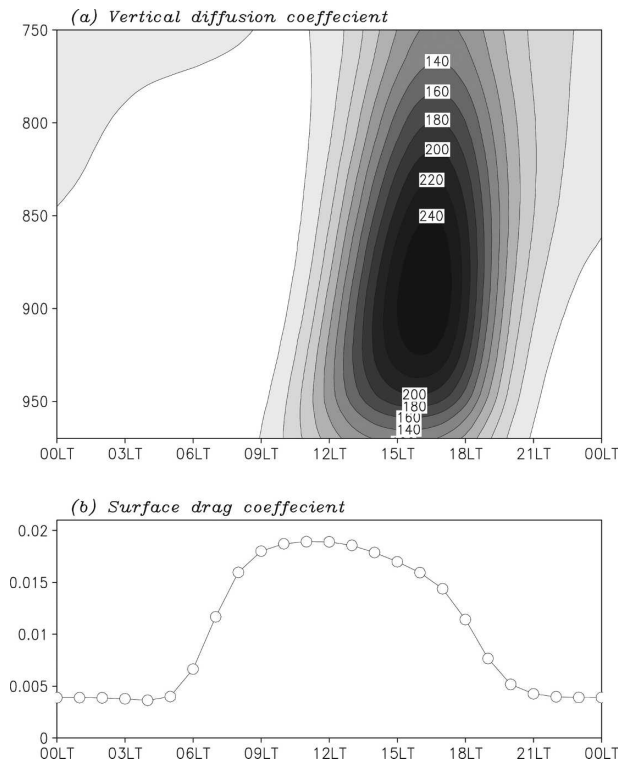
FIG. 7. Vertical distributions of the diurnal variation of (a) the vertical diffusion coefficient ($m^2 s^{-1}$) and (b) surface drag coefficient based on the AGCM simulation. Both parameters are averaged over the box region shown in Fig. 1.

variation of the pressure gradient force and vertical diffusion have comparable magnitudes. To identify more clearly the roles of these two effects, we next conduct idealized experiments aimed at isolating their individual impacts on the diurnal wind changes.

b. Idealized model solution

Only the momentum equation is considered in our idealized model, which is based on Eq. (7) except that the residual term is not considered. The grid system in the idealized model follows that of the AGCM. The winds are initially set to be zero and a time step of 1 h is used for the integration. The diurnal evolution (at 1-h time intervals) of the three-dimensional pressure gradient force and vertical diffusion/surface drag coefficients at each grid point is obtained by computing climatological averages of the AGCM output. The vertical diffusion term is calculated with an implicit scheme similar to that used in the AGCM, so as to ensure stability of the integrations. Note that different horizontal points do not communicate with each other.

This simple model has been integrated for 10 days to obtain a regular wind diurnal oscillation. The diurnal evolution of winds during the last 30 h is displayed in

Fig. 8. The lhs (rhs) of this figure portrays the diurnal evolution of vertical (latitudinal) structures of the meridional wind. The evolution of the wind simulated by the AGCM is provided in Fig. 8a to facilitate comparison with the simple model results. All results shown here for both the AGCM and simple model experiments are defined on the model sigma levels. For the vertical distributions, the wind data are averaged over the box region shown in Fig. 1. The latitudinal distributions of the winds on the rhs are taken from the sixth model level from the surface (about 900 mb) and are averaged over 100°–95°W. The diurnal evolution of the vertical profile shown in Fig. 8a is analogous to that in Fig. 4b, except that the results presented in Fig. 4b have been interpolated to the pressure levels. The pattern on the rhs of Fig. 8a suggests that the meridional wind attains maximum amplitude at about the same time over the range of latitudes between 30° and 45°N.

In the first experiment (PG) with the simple model, the vertical diffusion/surface drag coefficients are set to their corresponding daily mean. This case is aimed at examining the mechanism proposed by Holton (1967), as discussed earlier. The results are displayed in Fig. 8b. A clear diurnal oscillation of the meridional wind is evident in both the vertical and latitudinal profiles. However, as shown in the vertical profile (lhs), the domain-averaged maximum wind occurs near midnight, about 2 h earlier than the peak as simulated in the AGCM. The wind amplitude is noticeably weaker than that generated by the AGCM. Moreover, the latitudinal profile of the diurnal phase as shown on the rhs illustrates a distinct meridional phase shift. South of 35°N, the maximum diurnal phase occurs before midnight. The diurnal peak shifts to about 0600 LT to the north of 37°N. This latitudinal variation is in sharp contrast to the uniform meridional phase of the LLJ as simulated in the AGCM (Fig. 8a).

Next, we conduct another experiment (VDIF) by fixing the pressure gradient force at its daily mean value. This case is intended to isolate the effects of Blackadar's (1957) mechanism for the LLJ. A comparison of the vertical profile produced by this experiment (Fig. 8c) to that by the AGCM (Fig. 8a) reveals that the LLJ is relatively weaker in the absence of the diurnal variation of the pressure gradient force. The phase of the maximum wind in the lower PBL occurs at about 0600 LT, instead of 0200 LT as in the AGCM simulation. The wind maximum in this experiment (Fig. 8c, rhs) also exhibits a latitudinal shift. The earliest peak occurs at about 36°N. On both sides of this latitude, the phase of maximum wind is delayed by a few hours near 30° and 40°N.
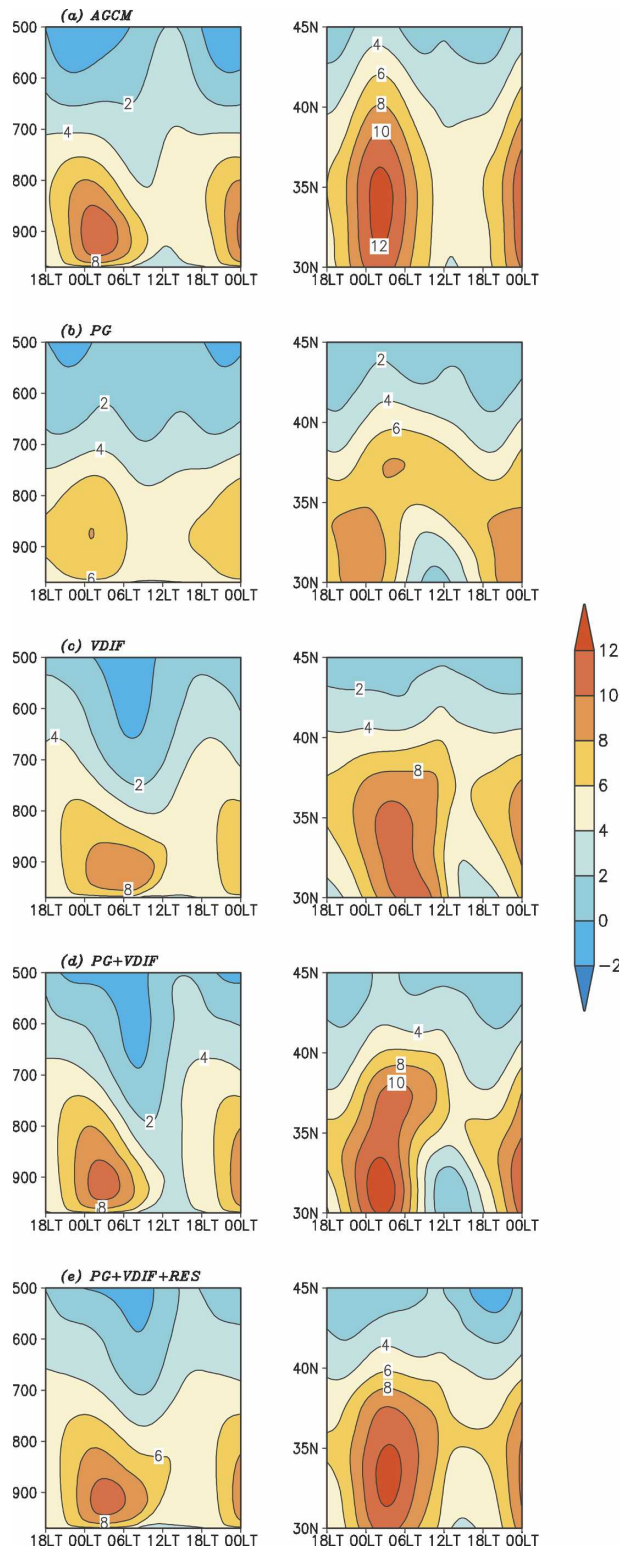
FIG. 8. Diurnal evolution of the vertical distribution (lhs; averaged over box region in Fig. 1) and horizontal structure at the sixth model level from the surface (rhs; averaged over 100°–95°W) of the meridional wind for (a) AGCM and experiments based on the simple models (b) PG, (c) VDIF, (d) PG + VDIF, and (e) PG + VDIF + RES (m s^{-1}).

In a third experiment (PG + VDIF), both the diurnal evolution of pressure gradient force and vertical diffusion are considered. It is readily seen that with consideration of both effects, the simple model generates a diurnal cycle with amplitude and phase structure (Fig. 8d) comparable to that in the AGCM simulation. The height of the maximum wind is close to that simulated by the AGCM (lhs). More interestingly, the meridional phase shift as noticed in the PG and VDIF experiments is reduced considerably (Fig. 8d, rhs), although a slight phase shift is still discernible to the north of 35°N. Additionally, the maximum wind in this experiment is located at 32°N instead of 34°N in the AGCM simulation.

The residual term (IV) in Eq. (7) is not considered in the PG + VDIF experiment. Some of the discrepancies between Figs. 8a and 8d could be attributed to the lack of horizontal communication resulting from the neglect of horizontal advection and horizontal diffusion terms in this experiment. To further check this point, another experiment has been conducted with the residual term (as computed using AGCM output) being included in the forcing, together with the pressure gradient force and vertical diffusion. The results of this experiment (PG + VDIF + RES), shown in Fig. 8e, illustrate that although the magnitude of the residual term is relatively small, the simulation is much improved by including this term. In particular, the uniform meridional diurnal phase and the location of the LLJ center at 34°N are well captured by this experiment.

Results from the above experiments indicate that although the mechanisms proposed by Holton (1967) and Blackadar (1957) for the formation of the LLJ can generally explain the diurnal oscillation with maximum meridional wind during the night, each of these mechanisms does not fully account for the detailed characteristics of the observed LLJ. Particularly, the LLJ generated by either mechanism exhibits an unrealistic meridional phase shift. Additional experiments (figures not shown) suggest that this latitudinal phase shift in both PG and VDIF experiments is due mainly to the latitudinal variation of the meridional component of pressure gradient force. To illustrate this effect in the PG experiment, the latitudinal changes in the diurnal evolution of the perturbation pressure gradient force at the sixth model level (about 900 mb) during the afternoon and earlier evening is shown in Fig. 9a. As in the calculations for the rhs of Fig. 8, data displayed in Fig. 9a are also averaged over the longitudes between 100° and 95°W. The pressure gradient force is primarily directed westward south of 35°N and southwestward farther north. Considering the wind tendency driven by this perturbation pressure gradient force, as well as the clockwise rotation of the wind vector accompanying the
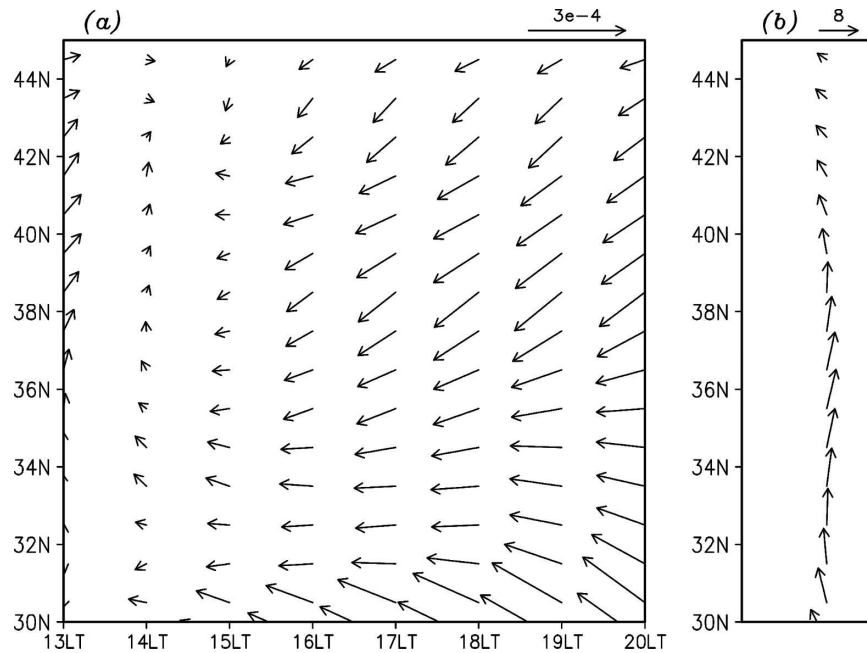
FIG. 9. Latitudinal distribution of (a) the time evolution of the perturbation horizontal pressure gradient force in the afternoon [see scale at upper rhs (m s^{-1})] and of (b) summer mean wind vectors [scale at top (m s^{-1})]. The variables in both (a) and (b) are from the sixth model level from the surface and averaged over 100°–95°W.

inertial oscillation, the wind south of 35°N would attain a maximum southerly component at an earlier time than that at higher latitudes (Fig. 8b, rhs). Further inspection shows that the meridional distribution of the perturbation pressure gradient force as shown in Fig. 9a is associated with a negative perturbation pressure center around 33°N during late afternoon and early evening. This negative perturbation pressure center is found to be related to the westward-propagating diurnal tidal signal.

In the VDIF experiment, the diurnal oscillation of wind is triggered by the reduction in vertical mixing at sunset; however, the phase of oscillation is strongly dependent on the orientation of the local mean flow. To understand the latitudinal shift of the maximum LLJ in this experiment, the meridional profile of daily mean wind vectors is illustrated in Fig. 9b. The mean wind has the largest eastward component at 36°N. For regions north/south of this latitude, the wind vectors exhibit an anticlockwise turning; they are directed northward at 39° and 33°N and northwestward farther north/south. Considering that the diurnal evolution of vertical diffusion/surface drag coefficients is largely in the same phase over these latitudes, the inertial oscillation associated with this meridional profile of mean wind would lead to the earliest appearance of a maximum northward component at 36°N (see Fig. 8c, rhs). This meridi-

onal profile of mean wind is controlled by the mean pressure gradient pattern, which is further closely related to the local terrain (the highest peak of the Rockies is located at around 39°N; see Fig. 6). Also note that a change of the inertial oscillation period with latitudes would also contribute to the latitudinal shift of the maximum LLJ in both PG and VDIF experiments to some degree.

c. Vertical phase tilt of the LLJ

Another interesting feature of the LLJ is that the peak phase of the wind exhibits a vertical tilt in the PBL, as clearly shown in the AGCM simulation in Fig. 8a (lhs). In the lower PBL, the maximum of southerly wind occurs at 0200 LT, while the peak wind speed is attained earlier in the upper PBL at 2200 LT near 800 mb. A clear phase shift with altitude of the LLJ has also been illustrated by Higgins et al. (1997) with wind profiler observation at 36°N, 97.5°W (their Fig. 5) and by Krishna (1968) based on simple model simulation and station observations. Note that in the PG experiment, the vertical phase tilt is not clearly evident (Fig. 8b, lhs). In contrast, in the VDIF experiment, a clear vertical tilt is discernible (Fig. 8c). Therefore the vertical phase tilt of the LLJ in the PBL appears to be closely associated with the diurnal variation of vertical mixing coeffi-
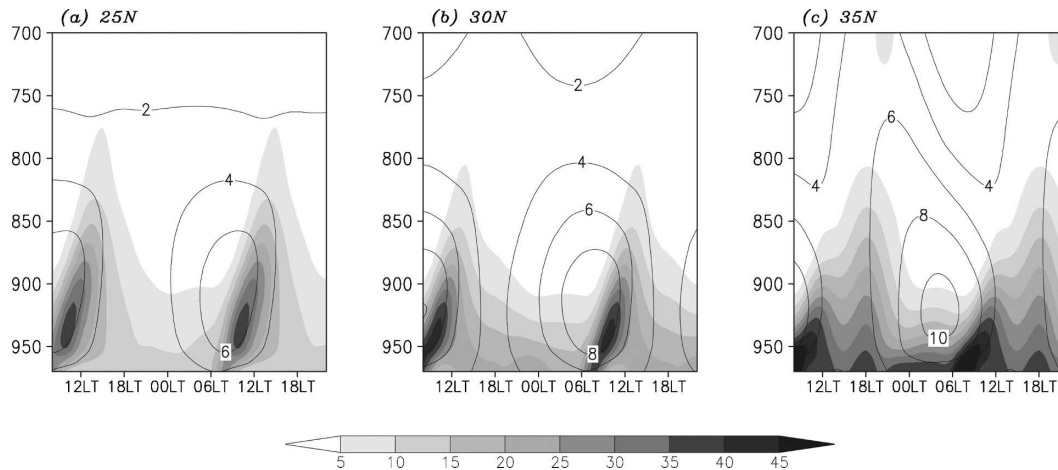
FIG. 10. Vertical distribution of the diurnal evolution of the meridional wind [contours (m s^{-1})] and amplitude of vertical diffusion (diff = $\sqrt{\text{diff}_x^2 + \text{diff}_y^2}$; shading; see bar scale at bottom (10^5 m s^{-1})] at (a) 25°, (b) 30°, and (c) 35°N for the VDIF experiment. All fields are averaged over 100°–95°W.

cients. Furthermore, Krishna (1968) noted that the vertical phase tilt of the LLJ is dependent on latitudes, with negative tilt (upper level leads lower level) at latitudes north of 30°N, zero tilt around 30°N, and positive tilt (upper level lags lower level) south of 30°N. Considering that the most important characteristics of the vertical phase tilt in the AGCM simulation are largely captured in VDIF, we will focus on the results based on this experiment in the following discussion.

The diurnal evolution of the meridional wind (contours) with height at three different latitudes (25°, 30°, and 35°N) in VDIF is displayed in Fig. 10. The phenomenon described by Krishna (1968) is reproduced in this figure. The phase tilt is most obvious at 35°N. It becomes weaker at 30°N. A tilt in the opposite direction is seen at 25°N.

The diurnal evolution of the vertical profile of the magnitude of the vertical diffusion is shown in Fig. 10 (shading). At 35°N (Fig. 10c), it is seen that strong vertical mixing persists longer in the lower than in the upper PBL; that is, the frictional drag on the flow is relaxed in a sequential fashion from the top of the PBL downward after sunset. Sensitivity tests indicate that the vertical phase tilt of the LLJ is largely caused by this sequential diminution of the frictional drag from the upper to lower PBL. As a result, the strength of the airflow in the upper PBL peaks at an earlier hour than that in the lower PBL.

For the 30°N case (Fig. 10b), the shape of the diurnal evolution of vertical diffusion is similar to that at 35°N. However, due to the change of orientation of prevailing mean wind as previously mentioned and the longer inertial oscillation period at this latitude, it takes longer to reach the maximum southerly wind. In the lower

PBL, the inertial oscillation tends to yield a maximum southerly peak after sunrise, by which time strong vertical mixing resumes. Therefore, the inertial oscillation is interrupted before this southerly peak can be realized. Instead, the actual maximum meridional wind in the lower PBL tends to occur just before strong vertical mixing sets in. In the upper PBL, the inertial oscillation still has sufficient time to evolve to the southerly LLJ peak. Thus, the vertical phase tilt of the LLJ originally triggered at sunset will be weakened by the resumption of strong vertical diffusion at the lower PBL after sunrise. For the 25°N case (Fig. 10a), the modulation of the inertial oscillation in the lower PBL by the vertical mixing is even stronger than that at 30°N because of the even longer inertial oscillation period. Consequently, the phase tilt is further weakened, and there is even a slight hint of a tilt in the opposite direction in Fig. 10a.

5. Summary and discussion

In this study, the fidelity of the LLJ simulated by the GFDL AGCM is assessed by comparison with the North American Regional Reanalysis. Results show that the AGCM captures the most prominent features of the LLJ, including its horizontal/vertical structure as well as its diurnal phase and amplitude. A diagnosis based on the AGCM simulation is conducted to evaluate various physical mechanisms for the formation of the LLJ. The diurnal variation of the pressure gradient force and vertical diffusion are both important in regulating the inertial oscillation and in determining the diurnal phase of the LLJ. These two mechanisms, as proposed by Holton (1967) and Blackadar (1957), yield diurnal wind oscillations with comparable amplitudes.

A simple model is constructed to further understand the relative roles of these two mechanisms. In such idealized experiments, the diurnal variation of pressure gradient force and vertical diffusion coefficients are computed using output from the AGCM. The results from these experiments illustrate that Holton's or Blackadar's theory alone does not account for certain detailed features of the LLJ appearing in the AGCM. The amplitude of the LLJ forced by either mechanism is weaker than that simulated by the AGCM, and the phase of maximum wind exhibits unrealistic meridional shifts. This meridional phase shift is found to be associated with the latitudinal variation of the pressure gradient force.

The temporal phase of the LLJ exhibits a notable tilt with height in the PBL. This vertical tilt is more obvious near 35°N, where the wind in the upper PBL attains a southerly peak several hours earlier than that in the lower PBL. This tilt is reduced in lower latitudes. At 25°N, the tilt becomes rather weak or even reverses. Our numerical experiments based on the simple model demonstrate that this vertical tilt is primarily caused by an earlier cessation of strong vertical mixing in the upper PBL relative to that in the lower PBL. As a result, the wind in the upper PBL reaches maximum strength prior to the signal in the lower PBL. In the lower latitudes, however, due to the change of the orientation of prevailing mean wind vectors and the longer inertial oscillation period, the inertial oscillation in the lower PBL is interrupted by strong vertical mixing the following morning.

All results discussed above regarding the features of and mechanisms for the LLJ are based on the climatological diurnal cycle of the LLJ. Thus, we cannot rule out the importance of other mechanisms in affecting the LLJ behavior in some particular cases. For instance, Uccellini and Johnson (1979) proposed that the upper-level jet could exert an influence on the low-level jet during some LLJ events.

As noted in the introduction, the nocturnal LLJ plays an important role in modulating the diurnal cycle of rainfall over the Great Plains via moisture transport or low-level convergence. The intimate relationship between the LLJ and rainfall is also verified using the NARR data. Figure 11a illustrates the climatological summertime rainfall pattern over the U.S. continent at 0300 LT. The most significant feature in this pattern is the strong rainfall maximum over the Great Plains, whereas much lighter rainfall is observed over southeastern United States and the North American monsoon region (i.e., southwest United States and Mexico). The rainfall in the latter regions peaks in the local af-
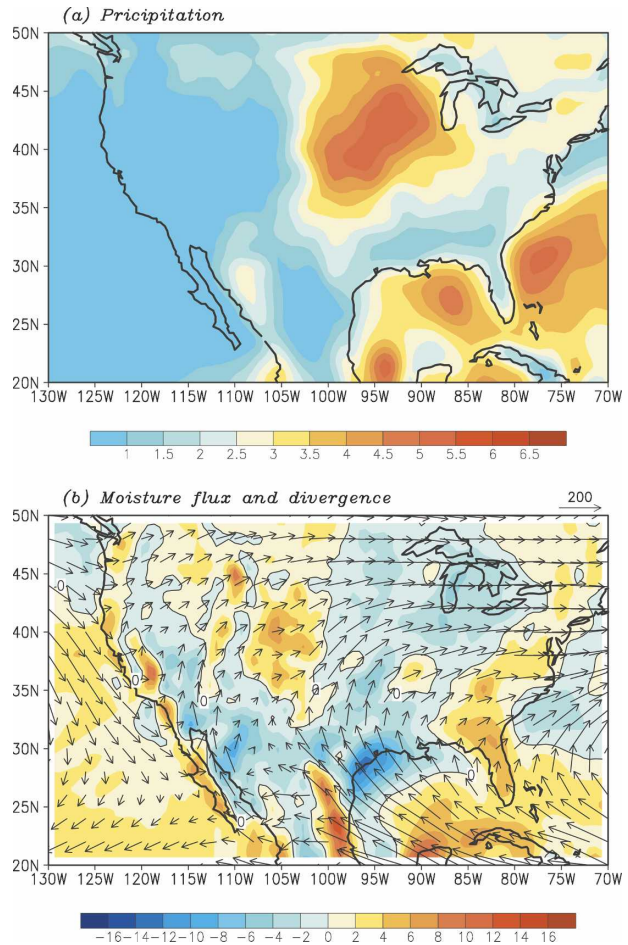

FIG. 11. Climatological distribution at 0300 LT of the summertime (a) rainfall (mm day^{-1}) and (b) vertically integrated moisture flux [arrows; scale at upper rhs (m s^{-1} g kg^{-1})] and divergence [shading; see scale at bottom (mm day^{-1})]. All fields are based on NARR data.

ternoon–early evening. The pattern in Fig. 11a also shows rainfall maxima on both sides of the Florida Peninsula. The rainfall center over the Great Plains is seen to be coincident with vertically integrated moisture convergence at 0300 LT (shading in Fig. 11b). The vertically integrated moisture flux pattern (arrows in Fig. 11b) indicates that this nocturnal moisture convergence over the Great Plains is mainly associated with two branches of moisture transport: a mid- and upper-tropospheric branch originating from the western United States at about 45°N and a low-tropospheric branch directed from the Gulf of Mexico (i.e., the LLJ). The results in the altitude of these two branches (not shown) are consistent with the analysis by Helfand and Schubert (1995) and Higgins et al. (1997), and further confirm the important role of the LLJ in supporting the nocturnal rainfall peak in the Great Plains.

However, it is worth noting that although the essential features of the LLJ are successfully captured by the GFDL AGCM, the simulation of the diurnal cycle of rainfall over the Great Plains by this AGCM is relatively poor. The AGCM produces an afternoon rainfall peak over this region instead of a nocturnal one. Similar AGCM deficiencies are also found in other AGCMs (e.g., Lee et al. 2007). These results suggest that the simulation of the LLJ is a necessary but insufficient condition for correctly simulating the nocturnal precipitation in the Great Plains. Further diagnosis based on the AGCM simulation indicates that the lack of the eastward-migrating convective signal from the Rockies into the Great Plains (e.g., Carbone et al. 2002) could be a probable cause for the model deficiencies in reproducing the observed rainfall pattern over this region. Nonetheless, by expanding our knowledge of the mechanisms for the LLJ, the present study is a useful step toward a better understanding and simulation of the climate system in North America during the warm season.

REFERENCES

Astling, E. G., J. Paegle, E. Miller, and C. J. O'Brien, 1985: Boundary layer control of nocturnal convection associated with a synoptic-scale system. *Mon. Wea. Rev.,* **113,** 540–552.

Beljaars, A. C. M., 1995: The parameterization of surface-fluxes in large-scale models under free convection. *Quart. J. Roy. Meteor. Soc.,* **121,** 255–270.

Benton, G. S., and M. A. Estoque, 1954: Water-vapor transfer over the North American continent. *J. Meteor.,* **11,** 462–477.

Blackadar, A. K., 1957: Boundary layer wind maxima and their significance for the growth of nocturnal inversions. *Bull. Amer. Meteor. Soc.,* **38,** 283–290.

Bleeker, W., and M. J. Andre, 1951: On the diurnal variation of precipitation, particularly over central U.S.A., and its relation to large-scale orographic circulation systems. *Quart. J. Roy. Meteor. Soc.,* **77,** 260–271.

Bonner, W. D., 1968: Climatology of the low-level jet. *Mon. Wea. Rev.,* **96,** 833–850.

——, and J. Paegle, 1970: Diurnal variations in the boundary layer winds over the south-central United States in summer. *Mon. Wea. Rev.,* **98,** 735–744.

Carbone, R. E., J. D. Tuttle, D. A. Ahijevych, and S. B. Trier, 2002: Inferences of predictability associated with warm season precipitation episodes. *J. Atmos. Sci.,* **59,** 2033–2056.

Fast, J. D., and M. D. McCorcle, 1990: A two-dimensional numerical sensitivity study of the Great Plains low-level jet. *Mon. Wea. Rev.,* **118,** 151–163.

Frisch, A. S., B. W. Orr, and B. E. Martner, 1992: Doppler radar observations of the development of a boundary-layer nocturnal jet. *Mon. Wea. Rev.,* **120,** 3–16.

GFDL Global Atmospheric Model Development Team, 2004: The new GFDL global atmosphere and land model AM2-LM2: Evaluation with prescribed SST simulations. *J. Climate,* **17,** 4641–4673.

Helfand, H. M., and S. D. Schubert, 1995: Climatology of the Great Plains low-level jet and its contribution to the continental moisture budget of the United States. *J. Climate,* **8,** 784–806.

Hering, W. S., and T. R. Borden, 1962: Diurnal variations in the summer wind field over the central United States. *J. Atmos. Sci.,* **19,** 81–86.

Higgins, R. W., Y. Yao, E. S. Yarosh, J. E. Janowiak, and K. C. Mo, 1997: Influence of the Great Plains low-level jet on the summertime precipitation and moisture transport over the central United States. *J. Climate,* **10,** 481–507.

Hoecker, W. H., Jr., 1963: Three southerly low-level jet systems delineated by the Weather Bureau special pibal network of 1961. *Mon. Wea. Rev.,* **91,** 573–582.

——, 1965: Comparative physical behavior of southerly boundary layer jets. *Mon. Wea. Rev.,* **93,** 133–144.

Holton, J. R., 1967: The diurnal boundary layer wind oscillation above sloping terrain. *Tellus,* **19,** 199–205.

Izumi, Y., and M. L. Barad, 1963: Wind and temperature variations during development of a low-level jet. *J. Appl. Meteor.,* **2,** 668–673.

Klein, S. A., X. Jiang, J. Boyle, S. Malyshev, and S. Xie, 2006: Diagnosis of the summertime warm and dry bias over the U.S. Southern Great Plains in the GFDL climate model using a weather forecasting approach. *Geophys. Res. Lett.,* **33,** L18805, doi:10.1029/2006GL027567.

Krishna, K., 1968: A numerical study of the diurnal variation of meteorological parameters in the planetary boundary layer. Part I: Diurnal variations of winds. *Mon. Wea. Rev.,* **96,** 269–276.

Lee, M.-I., and Coauthors, 2007: An analysis of the warm season diurnal cycle over the continental United States and northern Mexico in general circulation models. *J. Hydrometeor.,* in press.

Lock, A. P., 1998: The parameterization of entrainment in cloudy boundary layers. *Quart. J. Roy. Meteor. Soc.,* **124,** 2729–2753.

——, A. R. Brown, M. R. Bush, G. M. Martin, and R. N. B. Smith, 2000: A new boundary layer mixing scheme. Part I: Scheme description and single-column model tests. *Mon. Wea. Rev.,* **128,** 3187–3199.

Louis, J.-F., 1979: A parametric model of vertical eddy fluxes in the atmosphere. *Bound.-Layer Meteor.,* **17,** 187–202.

Maddox, R. A., 1980: Mesoscale convection complexes. *Bull. Amer. Meteor. Soc.,* **61,** 1374–1387.

McCorcle, M. D., 1988: Simulation of surface-moisture effects on

the Great Plains low-level jet. *Mon. Wea. Rev.,* **116,** 1705–1720.

McNider, R. T., and R. A. Pielke, 1981: Diurnal boundary-layer development over sloping terrain. *J. Atmos. Sci.,* **38,** 2198–2212.

Means, L. L., 1952: On thunderstorm forecasting in the central United States. *Mon. Wea. Rev.,* **80,** 165–189.

——, 1954: A study of the mean southerly wind—Maximum in low levels associated with a period of summer precipitation in the Middle West. *Bull. Amer. Meteor. Soc.,* **35,** 166–170.

Mesinger, F., and Coauthors, 2006: North American Regional Re-analysis. *Bull. Amer. Meteor. Soc.,* **87,** 343–360.

Mitchell, M. J., and R. A. Arritt, 1995: An hourly climatology of the summertime Great Plains low-level jet using wind profiler observations. *Wea. Forecasting,* **10,** 576–591.

Moorthi, S., and M. J. Suarez, 1992: Relaxed Arakawa–Schubert: A parameterization of moist convection for general circulation models. *Mon. Wea. Rev.,* **120,** 978–1002.

Paegle, J., and D. W. McLawhorn, 1983: Numerical modeling of diurnal convergence oscillations above sloping terrain. *Mon. Wea. Rev.,* **111,** 67–85.

Parish, T. R., A. R. Rodi, and R. D. Clark, 1988: A case study of the summertime Great Plains low level jet. *Mon. Wea. Rev.,* **116,** 94–105.

Pitchford, K. L., and J. London, 1962: The low-level jet as related to nocturnal thunderstorms over Midwest United States. *J. Appl. Meteor.,* **1,** 43–47.

Rasmusson, E. M., 1967: Atmospheric water vapor transport and the water balance of North America. Part I: Characteristics of the water vapor flux field. *Mon. Wea. Rev.,* **95,** 403–426.

——, 1968: Atmospheric water vapor transport and the water balance of North America. Part II: Large-scale water balance investigations. *Mon. Wea. Rev.,* **96,** 720–734.

Ting, M., and H. Wang, 2006: The role of the North American topography on the maintenance of the Great Plains summer low-level jet. *J. Atmos. Sci.,* **63,** 1056–1068.

Uccellini, L. W., and D. R. Johnson, 1979: The coupling of upper and lower tropospheric jet streams and implications for the development of severe convective storms. *Mon. Wea. Rev.,* **107,** 682–703.

Wallace, J. M., 1975: Diurnal variations in precipitation and thun-derstorm frequency over the conterminous United States. *Mon. Wea. Rev.,* **103,** 406–419.

Wexler, H., 1961: A boundary layer interpretation of the low level jet. *Tellus,* **13,** 368–378.

Zhong, S., J. D. Fast, and X. Bian, 1996: A case study of the Great Plains low-level jet using wind profiler network data and a high-resolution mesoscale model. *Mon. Wea. Rev.,* **124,** 785–806.